

# Two-Sample Testing with Block-Wise Missingness in Multi-Source Data

Kejian Zhang<sup>1</sup>, Muxuan Liang<sup>2</sup>, Robert Maile<sup>3</sup>, Doudou Zhou<sup>1,†</sup>

<sup>1</sup>Department of Statistics and Data Science, National University of Singapore, Singapore

<sup>2</sup>Department of Biostatistics, University of Florida, USA

<sup>3</sup>Department of Surgery, College of Medicine, University of Florida, USA

<sup>†</sup>Corresponding author: ddzhou@nus.edu.sg

## Abstract

Multi-source and multi-modal datasets are increasingly common in scientific research, yet they often exhibit *block-wise missingness*, where entire data sources or modalities are systematically absent for subsets of subjects. This structured form of missingness presents significant challenges for statistical analysis, particularly for two-sample hypothesis testing. Standard approaches such as imputation or complete-case analysis can introduce bias or result in substantial information loss, especially when the missingness mechanism is not random. To address this methodological gap, we propose the Block-Pattern Enhanced Test (BPET), a general framework for two-sample testing that directly accounts for block-wise missingness without requiring imputation or deletion of observations. As a concrete instantiation, we develop the Block-wise Rank In Similarity graph Edge-count (BRISE) test, which extends rank-based similarity graph methods to settings with block-wise missing data. Under mild conditions, we establish that the null distribution of BRISE converges to a  $\chi^2$  distribution. Simulation studies show that BRISE consistently controls the type I error rate and achieves good statistical power under a wide range of alternatives. Applications to two real-world datasets with block-wise missingness further demonstrate the practical utility of our method in identifying meaningful distributional differences.

*Keywords:* Nonparametric test; Multi-modality data; Rank-based methods; Graph-based statistics; High-dimensional inference.

# 1 Introduction

Multi-source and multi-modal datasets are increasingly common in scientific research, encompassing diverse data types collected across individuals, institutions, and time. Examples include the Alzheimer’s Disease Neuroimaging Initiative (ADNI) (Mueller et al., 2005a,b), which combines imaging, genetic, and clinical data, and electronic health records (EHRs) (Johnson et al., 2023) that integrate medication histories and clinical notes.

While such integration enables more powerful and comprehensive analyses, it also poses challenges related to data quality and structure. A key issue is *block-wise missingness*, where entire data sources are absent for certain individuals (Figure 1). This often stems from clinical priorities, resource constraints, or institutional protocols. For instance, in ADNI, site-level practices can produce systematic gaps across modalities (Xue and Qu, 2021). Similar patterns appear in partial or incomplete multi-view learning (Li et al., 2014; Xu et al., 2015; Zhao et al., 2016; Zhang et al., 2020; Zhou et al., 2023), such as bilingual document clustering with missing translations or audiovisual tasks where only one modality is available.

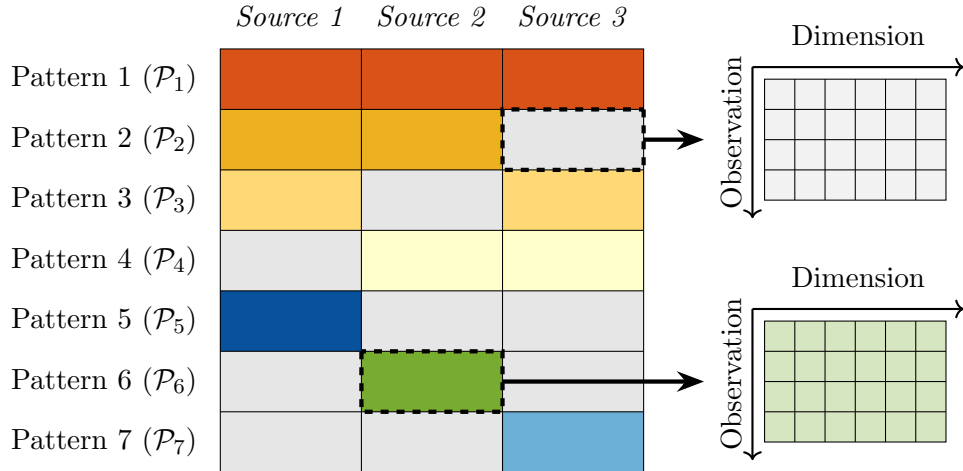


Figure 1: Pattern partition across three sources, with gray blocks indicating missing data. Seven nonempty patterns are shown: Pattern 1 is fully observed; Patterns 2–4 each have one missing source; Patterns 5–7 each have two missing sources.

These challenges are especially acute in the context of two-sample testing, a fundamental task in statistics that seeks to determine whether two groups are drawn from the same

distribution. Block-wise missingness introduces structural differences in data availability across groups that can distort analysis and bias conclusions. Formally, let  $X_1, \dots, X_m \stackrel{i.i.d}{\sim} F_X$  and  $Y_1, \dots, Y_n \stackrel{i.i.d}{\sim} F_Y$  be two independent samples. The goal is to test

$$H_0 : F_X = F_Y \quad \text{versus} \quad H_a : F_X \neq F_Y.$$

When the data are fully observed, many powerful nonparametric methods exist, including graph-based tests (Friedman and Rafsky, 1979; Schilling, 1986; Henze, 1988; Rosenbaum, 2005; Chen and Zhang, 2013; Chen and Friedman, 2017; Chen et al., 2018; Zhou and Chen, 2023), classification-based tests (Lopez-Paz and Oquab, 2017; Kim et al., 2021; Hediger et al., 2022), interpoint distance-based tests (Biswas and Ghosh, 2014; Li, 2018), and kernel-based tests (Gretton et al., 2006; Eric et al., 2007; Gretton et al., 2009, 2012; Song and Chen, 2024). These approaches exploit ranks, distances, or reproducing kernel Hilbert space (RKHS) embeddings to characterize distributional differences and are effective in high-dimensional or non-Euclidean settings where parametric models are not feasible.

However, nonparametric tests for missing data are sparse; naive implementation of existing methods leads to inflated type I error or unsatisfied power. Figure 2 summarizes existing strategies using imputation, complete-case, or available-case analysis. Specifically, imputation method fills in missing entries using model-based predictions (Toutenburg, 1990; Zhang, 2016) but relies on strong assumptions and can bias inference if those assumptions fail. Complete-case analysis discards incomplete samples, which reduces effective sample size (Little, 1992; Ross et al., 2020). Available-case analysis uses only variables required for a given comparison but can still suffer information loss and inefficiency (Little, 1992).

Recent work has extended classical two-sample testing procedures to handle entrywise missingness, but these approaches are often conservative under block-wise missingness. For example, MMD-Miss (Zeng et al., 2024a) and the univariate rank-based test of Zeng et al. (2024b) adopted bounding strategies that embed incomplete observations and construct finite upper and lower bounds for the maximum mean discrepancy (MMD) statistic (Gretton et al., 2012) and the Wilcoxon–Mann–Whitney statistic, respectively. The null is rejected only when both bounds fall in the rejection region, ensuring type I error control despite missing entries. In addition, Aleksić and Milošević (2025) proposes a weighted modification of the energy test statistic that leverages all available data under missingness. These approaches

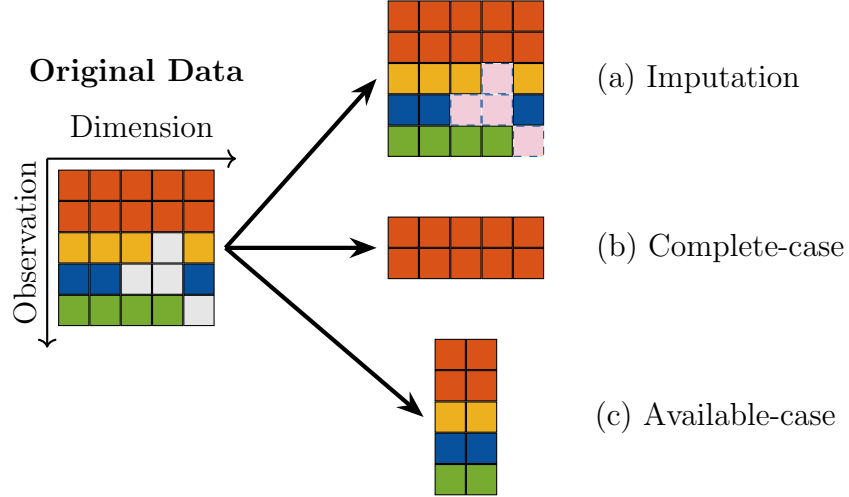


Figure 2: Three common strategies for handling missing data (gray entries).

perform well for random missing, but they do not target structured block-wise mechanisms.

To fill the gap, we propose the **Block-Pattern Enhanced Test** (BPET), a general framework for two-sample testing under block-wise missing data. BPET partitions the dataset by missingness patterns, applies pattern-aware procedures to each compatible pattern pair using shared observed sources, and aggregates the results into a global test statistic. This framework allows BPET to directly operate on partially observed data without imputation or case deletion. Further, in our proposed framework, many testing methods can be chosen as the test statistic; in this paper, we focus on a graph and rank-based instantiation on the Rank In Similarity graph Edge-count (RISE) test (Zhou and Chen, 2023). We call this method the **Block-wise Rank In Similarity graph Edge-count** (BRISE) test, which adapts rank-weighted similarity graphs to block-wise missingness. In our implementation, we adopt the permutation-based inference to construct the null distribution of the test statistics. Unlike the standard permutation, which shuffles all labels while fixing only the total group sizes, we introduce a *pattern-wise permutation* that restricts permutations within each pattern and we derive a sufficient condition for its validity that is strictly weaker than missing completely at random (MCAR). In theory, under mild regularity conditions, we establish that the BRISE statistics have asymptotic  $\chi^2$  null distributions. We also show that standard permutation can fail when the groups have unequal marginal pattern distributions. In simulations, BRISE maintains type I error control and achieves higher power than existing

competitors; in two empirical studies, BRISE detects meaningful distributional differences.

In summary, our contributions are threefold. First, we introduce BPET, a general framework that conducts two-sample testing directly on partially observed multi-source data without imputation or case deletion. Second, we propose a pattern-wise permutation scheme and addresses a failure mode of standard permutation. Third, we instantiate BPET via BRISE, develop its asymptotic theory, and demonstrate competitive empirical performance in simulations and real applications.

The remainder of the paper is organized as follows. Section 2 presents BPET and the proposed tests. Section 3 develops the theoretical properties. Sections 4 and 5 report simulation results and real data analyses. Section 6 concludes, with proofs and additional results in the Supplementary Materials.

## 2 Method

In this section, we first introduce the general framework and procedure of BPET in Section 2.1, then its adaptation to the RISE method in Section 2.2, and the construction of the test statistics tailored for block-wise missing data in Section 2.3.

### 2.1 Framework of Block-Pattern Enhanced Test (BPET)

**Stage 1: Pattern Partition.** Suppose there are  $L$  sources, indexed by  $l = 1, \dots, L$ , where each source is defined over a domain  $\mathcal{S}^{(l)}$ . These domains may vary across sources. For example,  $\mathcal{S}^{(l)}$  could be a Euclidean space such as  $\mathbb{R}^{d_l}$ , or a non-Euclidean space such as a network or a functional data space. Many real-world datasets, such as those from ADNI (Mueller et al., 2005a) described in Section 5.2, exhibit this multi-source structure by integrating diverse types of information, including imaging, genetic, and clinical measurements.

To accommodate block-wise missingness, let  $n_P$  denote the total number of distinct missingness patterns observed in the data. Each pattern is represented as

$$\mathcal{P}_\alpha = (P_\alpha^{(1)}, \dots, P_\alpha^{(L)}), \quad \alpha \in \{1, \dots, n_P\},$$

where  $P_\alpha^{(l)} = 1$  if source  $l$  is observed and 0 otherwise. For instance, when  $L = 3$ , Figure 1 shows that  $\mathcal{P}_1 = (1, 1, 1)$  corresponds to complete observation;  $\mathcal{P}_2 = (1, 1, 0)$ ,  $\mathcal{P}_3 = (1, 0, 1)$ ,

$\mathcal{P}_4 = (0, 1, 1)$  correspond to cases with two observed sources; and  $\mathcal{P}_5 = (1, 0, 0)$ ,  $\mathcal{P}_6 = (0, 1, 0)$ ,  $\mathcal{P}_7 = (0, 0, 1)$  correspond to cases with only one observed source. In general, the number of possible nonempty patterns is at most  $2^L - 1$ .

To unify our notations on two-sample problems, we introduce  $\{Z_i\}_{i=1}^N$  referring to all pooled observations, where  $\{Z_i\}_{i=1}^m = \{X_j\}_{j=1}^m$ ,  $\{Z_i\}_{i=m+1}^N = \{Y_j\}_{j=1}^n$ , and  $N = m + n$ . Thus, each observation can be written as  $Z_i = (Z_i^{(1)}, \dots, Z_i^{(L)})$ , where  $Z_i^{(l)} \in \mathcal{S}^{(l)}$  is the  $l$ -th source or modality if observed. Further, the missingness pattern of  $Z_i$  is  $S_i = (S_i^{(1)}, \dots, S_i^{(L)}) \in \{0, 1\}^L$ . Then the set of observations following pattern  $\mathcal{P}_\alpha$  is

$$\mathcal{Z}^{(\alpha)} = \{Z_i : S_i = \mathcal{P}_\alpha, 1 \leq i \leq N\}.$$

Based on the notations above, we define  $\mathcal{X}^{(\alpha)} = \mathcal{Z}^{(\alpha)} \cap \{X_i\}_{i=1}^m$  and  $\mathcal{Y}^{(\alpha)} = \mathcal{Z}^{(\alpha)} \cap \{Y_i\}_{i=1}^n$ , so that  $\mathcal{Z}^{(\alpha)} = \mathcal{X}^{(\alpha)} \cup \mathcal{Y}^{(\alpha)}$ . Let  $m_\alpha = |\mathcal{X}^{(\alpha)}|$ ,  $n_\alpha = |\mathcal{Y}^{(\alpha)}|$ , and  $N_\alpha = |\mathcal{Z}^{(\alpha)}|$ , where  $|\cdot|$  denotes the cardinality of a set. These satisfy

$$\sum_{\alpha=1}^{n_P} m_\alpha = m, \quad \sum_{\alpha=1}^{n_P} n_\alpha = n, \quad \sum_{\alpha=1}^{n_P} N_\alpha = \sum_{\alpha=1}^{n_P} (m_\alpha + n_\alpha) = N.$$

During this stage, we partition our observation from both samples based on their patterns, which facilitates the implementation of Stage 2.

**Stage 2: Pattern-aware Procedure.** Given the partitioned data, we define a *pattern pair* as  $(\mathcal{Z}^{(\alpha)}, \mathcal{Z}^{(\beta)})$  for  $1 \leq \alpha, \beta \leq n_P$ . For observations  $Z_i \in \mathcal{Z}^{(\alpha)}$  and  $Z_j \in \mathcal{Z}^{(\beta)}$ , if their patterns share at least one source (i.e.,  $\mathcal{P}_\alpha \mathcal{P}_\beta^\top > 0$ ), we define their dissimilarity as

$$\rho(Z_i, Z_j) = \text{Norm}\left(\sum_{l=1}^L S_i^{(l)} S_j^{(l)} \rho_l(Z_i^{(l)}, Z_j^{(l)})\right), \quad (1)$$

where  $\rho_l(\cdot, \cdot)$  is a source-specific dissimilarity measure and  $\text{Norm}(\cdot)$  is a normalization function. Notice that the dissimilarity between a pair of observations only uses the shared sources or modalities observed; we will discuss how to compute dissimilarity measure if no shared sources. There are many possible choices of the source-specific dissimilarity measure  $\rho_l(\cdot, \cdot)$ , which leads to different test-specific procedures. For Euclidean sources, one may take  $\rho_l(Z_i^{(l)}, Z_j^{(l)}) = \|Z_i^{(l)} - Z_j^{(l)}\|_2^2$  and  $\text{Norm}(x) = \sqrt{x}$ , which yields the Euclidean distance over the shared dimensions. The formulation in (1) is very flexible, which allows heterogeneous multi-modal data by choosing  $\rho_l(\cdot, \cdot)$  as, e.g., graph diffusion distances for networks

(Hammond et al., 2013), cosine similarities for embeddings (Kenter and De Rijke, 2015), or tailored measures for categorical data (Boriah et al., 2008). As an illustration, in Figure 1, given  $Z_i \in \mathcal{Z}^{(3)}$  and  $Z_j \in \mathcal{Z}^{(5)}$  with  $\mathcal{P}_3 = (1, 0, 1)$  and  $\mathcal{P}_5 = (1, 0, 0)$ , the only shared source is  $\mathcal{S}^{(1)}$ , and thus their dissimilarity is computed using only the first source or modality, which reduces to  $\rho(Z_i, Z_j) = \text{Norm}(\rho_1(Z_i^{(1)}, Z_j^{(1)}))$ .

If  $\mathcal{P}_\alpha \mathcal{P}_\beta^\top = 0$ , there are no shared sources, and direct computation of dissimilarity is impossible. We adopt a simple solution by assigning zero values to such pairs. While this takes the risk to discard potentially useful information, empirically it performs well in both simulation studies and real data analysis (Sections 4 and 5). We also explore an alternative method to define the dissimilarity among the non-overlapping pairs in Supplementary L.

Through Stage 2, for any pair of observations, we define and calculate their dissimilarities; these dissimilarities can be organized into a dissimilarity matrix, and partitioned following Stage 1 as a block-structured dissimilarity matrix, where each block corresponding to dissimilarities within a specific pattern pair.

**Stage 3: Test Statistic Assembly.** In Stage 3, the goal is to combine the block-structured dissimilarities from Stage 2 into a global test statistic for testing  $H_0$ . Because different pattern pairs may involve varying numbers and types of shared features, they can be on incompatible scales; directly applying existing two-sample methods to the full dissimilarity matrix may therefore lead to invalid conclusions. Section 2.3 presents two aggregation strategies designed to address this issue.

After aggregation, the global statistic is compared to its null distribution using a permutation-based procedure. This is non-trivial: standard permutation preserves only the overall group sizes and ignores the distribution of missingness patterns, which can inflate type I error when the groups differ in marginal pattern probabilities. To obtain valid inference in such settings, we propose a new permutation scheme tailored to block-wise missing data. We first specify the data-generating model and then define the relevant permutation distributions.

Let  $Z = (Z^{(1)}, \dots, Z^{(L)})$  denote the full data vector taking values in  $\prod_{l=1}^L \mathcal{S}^{(l)}$ , and let  $S \in \{0, 1\}^L$  denote the missingness pattern. For group  $g \in \{X, Y\}$ , the full data follow  $Z \sim F_g$  and the joint distribution of  $(Z, S)$  is

$$P_g(z, s) = P_g(S = s \mid Z = z) \frac{dF_g(z)}{dz}.$$

The observed data consist of  $(Z^{\text{obs}}, S)$ , where  $Z^{\text{obs}}$  is the subvector of  $Z$  indexed by  $\{l : S^{(l)} = 1\}$ . All test statistics are measurable functions of  $(Z^{\text{obs}}, S)$ . Our inference is carried out under the null hypothesis  $H_0 : F_X = F_Y$ , while allowing  $P_g(S = s \mid Z = z)$  to differ between groups.

**Definition 1** (Permutation distributions). *Let  $T = T(Z_1^{\text{obs}}, S_1, \dots, Z_N^{\text{obs}}, S_N; J_1, \dots, J_N)$  be a test statistic computed from the observed data  $(Z_i^{\text{obs}}, S_i)$  with group labels  $J_i \in \{X, Y\}$ .*

(i) *The standard permutation distribution of  $T$  is obtained by recomputing  $T$  after uniformly permuting the labels  $\{J_i\}$  over all  $\binom{N}{m}$  assignments with  $m$  labels  $X$  and  $n$  labels  $Y$ , keeping  $\{(Z_i^{\text{obs}}, S_i)\}$  fixed. Under  $H_0$ , this is called the permutation null distribution.*

(ii) *The pattern-wise permutation distribution is obtained by permuting the labels independently within each missingness pattern  $\mathcal{P}_\alpha$ , preserving  $(m_\alpha, n_\alpha)$ . Under  $H_0$ , this is called the pattern-wise permutation null distribution.*

Let  $\tilde{T} = T(Z_1^{\text{obs}}, S_1, \dots, Z_N^{\text{obs}}, S_N; \tilde{J}_1, \dots, \tilde{J}_N)$  with  $\tilde{J}_i \in \{X, Y\}$  denote the statistic recomputed under permutation. The following theorem establishes the failure of the standard permutation scheme when the groups differ in their marginal pattern distributions, with proof given in Supplementary A.

**Theorem 1** (Failure of standard permutation under unequal pattern distributions). *Suppose that for every pattern  $s$  with positive probability under both groups,*

$$F_X(\cdot \mid S = s) = F_Y(\cdot \mid S = s),$$

*but there exists at least one  $s$  such that  $P_X(S = s) \neq P_Y(S = s)$ . Then under  $H_0$ , the distributions of  $T$  and  $\tilde{T}$  differ when  $\{\tilde{J}_i\}$  are generated by the standard permutation scheme. Consequently,  $p$ -values based on the standard permutation distribution are invalid.*

Theorem 1 demonstrates that standard permutation can fail whenever the two groups differ in their marginal distribution of missingness patterns, even if their conditional distributions within each pattern are identical. In such cases,  $H_0$  may be rejected not because  $F_X \neq F_Y$ , but because of differences in the pattern distributions, leading to inflated type I error. This motivates restricting permutations to occur within patterns.



**Theorem 2** (Validity of pattern-wise permutation). *Let  $\tilde{T}$  denote the statistic computed using pattern-wise permutation. Under  $H_0 : F_X = F_Y$ , a sufficient condition for  $\tilde{T} \stackrel{d}{=} T$  is*

$$\frac{P_X(S = s \mid Z = z)}{P_X(S = s)} = \frac{P_Y(S = s \mid Z = z)}{P_Y(S = s)} \quad \text{for all } s \text{ with } P_g(S = s) > 0, g \in \{X, Y\}. \quad (2)$$

*This condition is strictly weaker than MCAR, which requires  $P_g(S = s \mid Z = z) = P_g(S = s)$  a.s.  $F_g$  for all  $s, g \in \{X, Y\}$ .*

The proof is given in Supplementary B. Condition (2) is strictly weaker than both MCAR and the requirement for validity of standard permutation: whenever either of those holds, pattern-wise permutation is also valid. To our knowledge, this is the first general criterion that guarantees the validity of permutation inference under block-wise missingness. Under Condition (2), labels are exchangeable within each pattern, and the pattern-wise permutation distribution coincides with the null distribution conditional on the missingness patterns.

In the remainder of the paper we assume that Condition (2) holds. BPET can be combined with a wide range of two-sample tests; Sections 2.2–2.3 develop its implementation within a graph-based framework tailored to block-wise missing data.

## 2.2 NNG-induced Rank

In this section, we incorporate the RISE method with the proposed BPET framework. RISE method uses the rank of observations; in this paper, we focus on the  $k$ -nearest neighbor graph (NNG)-induced ranking scheme. We first introduce the  $k$ -NNG-based rank construction in RISE, then describe its adaptation to pattern-wise settings in BPET framework.

There exist a number of non-parametric methods for two-sample testing, each have their strength on different types of data. RISE stands out as a powerful graph-based two-sample testing approach, utilizing ranks induced from the  $k$ -NNG or  $k$ -minimum spanning tree (MST) to construct the test statistic, which is more flexible when dealing with multiple types of data (or multiple modalities) simultaneously (Zhou and Chen, 2023). For simplicity, we focus on  $k$ -NNG in this paper since the test can be easily adjusted to other similarity graphs with the same theoretical properties.

**Definition 2** ( $k$ -NNG-induced Rank). *For any pair of observations  $(Z_i, Z_j)$ , compute their dissimilarity using (1) or other admissible metrics. The graph-induced rank of  $(Z_i, Z_j)$  is*

defined as

$$\text{rank}(Z_j \mid Z_i) = k + 1 - k',$$

if  $Z_j$  is the  $k'$ th nearest neighbor of  $Z_i$  for  $1 \leq k' \leq k$  and  $\text{rank}(Z_j \mid Z_i) = 0$  otherwise.

When ties occur in the dissimilarity values, the tied neighbors are assigned the average of the ranks they would otherwise occupy.

Now, we consider how to adapt RISE into the proposed BPET framework; the key idea is to define a systematic ranking scheme for any pattern-pairs. First, we define the (pattern) pair-wise  $k$ -NNG. Given two patterns  $\mathcal{P}_\alpha$  and  $\mathcal{P}_\beta$ , the pair-wise  $k$ -NNG is constructed based on observations from  $(\mathcal{Z}^{(\alpha)}, \mathcal{Z}^{(\beta)})$ , where each observation in  $\mathcal{Z}^{(\alpha)}$  is connected to its  $k$  nearest neighbors in  $\mathcal{Z}^{(\beta)}$ . An illustration of such pair-wise NNGs is shown in Figure 3. It is noteworthy that the structure of the  $k$ -NNG depends on the relationship between  $\mathcal{P}_\alpha$  and  $\mathcal{P}_\beta$ :

- If  $\alpha = \beta$ , then the  $k$ -NNG is a standard  $k$ -NNG, where edges may connect any pair of observations within the same pattern as depicted in the left panel of Figure 3.
- If  $\alpha \neq \beta$ , then the  $k$ -NNG is a bipartite graph, each observation in  $\mathcal{Z}^{(\alpha)}$  connects to its nearest neighbors in  $\mathcal{Z}^{(\beta)}$ , with no within-pattern edges as depicted in the right panel.

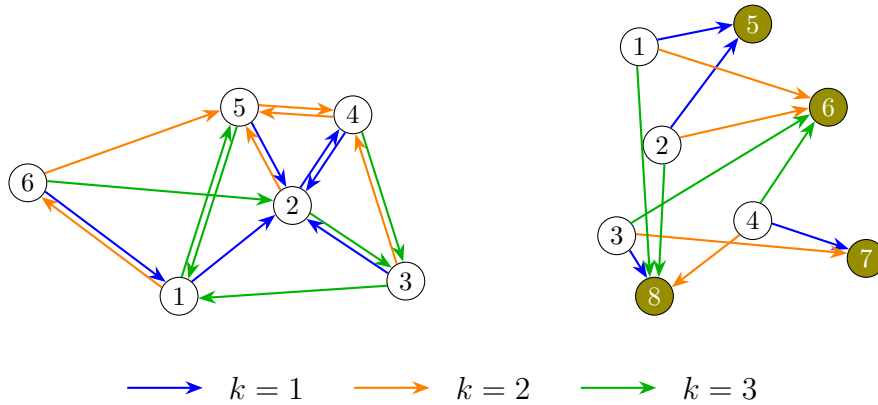


Figure 3: Example of  $k$ th-NNGs for  $(\mathcal{Z}^{(\alpha)}, \mathcal{Z}^{(\beta)})$  on two cases: Left panel shows the case when  $\alpha = \beta$ ; Right panel shows the case when  $\alpha \neq \beta$ , inducing a bipartite graph. Colors of arrows indicate neighbor level, while colors of nodes indicate observations from different patterns.

With the ranking scheme in Definition 2, the *rank of an observation*  $Z_j \in \mathcal{Z}^{(\beta)}$  with respect to  $Z_i \in \mathcal{Z}^{(\alpha)}$  is denoted by  $R_{ij}$ . The *total rank matrix* is then given by  $\mathbf{R} = [R_{ij}]_{i,j=1}^N$ . Grouping observations by missingness pattern, we denote  $\mathbf{R}(\mathcal{W}^{(\alpha)}, \mathcal{W}^{(\beta)}) = [R_{ij} : Z_i \in \mathcal{W}^{(\alpha)}, Z_j \in \mathcal{W}^{(\beta)}]$ ,  $\mathcal{W} \in \{\mathcal{X}, \mathcal{Y}, \mathcal{Z}\}$ . Then for  $(\mathcal{Z}^{(\alpha)}, \mathcal{Z}^{(\beta)})$ , the corresponding *pair-wise rank matrix* is defined as

$$\mathbf{R}^{(\alpha\beta)} = \mathbf{R}(\mathcal{Z}^{(\alpha)}, \mathcal{Z}^{(\beta)}) = \begin{bmatrix} \mathbf{R}(\mathcal{X}^{(\alpha)}, \mathcal{X}^{(\beta)}) & \mathbf{R}(\mathcal{X}^{(\alpha)}, \mathcal{Y}^{(\beta)}) \\ \mathbf{R}(\mathcal{Y}^{(\alpha)}, \mathcal{X}^{(\beta)}) & \mathbf{R}(\mathcal{Y}^{(\alpha)}, \mathcal{Y}^{(\beta)}) \end{bmatrix} = [R_{ij}^{(\alpha\beta)}]_{i,j=1}^{N_\alpha, N_\beta}.$$

When  $\mathcal{P}_\alpha \mathcal{P}_\beta^\top = 0$ , i.e., no shared sources (or modalities),  $\mathbf{R}^{(\alpha\beta)}$  would be a zero matrix.

## 2.3 Test Statistics

We now describe how to aggregate the pattern-pair level rank information into global test statistics. For simplicity, we adopt a symmetrized version of the rank matrix by setting  $\mathbf{R} \leftarrow \frac{1}{2}(\mathbf{R} + \mathbf{R}^\top)$ , which guarantees  $R_{ij}^{(\alpha\beta)} = R_{ji}^{(\beta\alpha)}$ . Throughout,  $\mathbf{R}$  denotes this symmetrized rank matrix.

For each pattern pair  $(\alpha, \beta)$ , define

$$U_x^{(\alpha\beta)} = \sum_{i=1}^{m_\alpha} \sum_{j=1}^{m_\beta} R_{ij}^{(\alpha\beta)}, \quad U_y^{(\alpha\beta)} = \sum_{i=1}^{n_\alpha} \sum_{j=1}^{n_\beta} R_{ij}^{(\alpha\beta)},$$

which represent the within-sample rank sums for groups  $X$  and  $Y$ . When  $\mathcal{P}_\alpha \mathcal{P}_\beta^\top = 0$ , dissimilarities are set to zero and the resulting ranks carry no information; such pairs are therefore excluded from the construction of test statistics. By symmetry,  $U_x^{(\alpha\beta)} = U_x^{(\beta\alpha)}$  and  $U_y^{(\alpha\beta)} = U_y^{(\beta\alpha)}$ .

Before defining the test statistics, we examine the behavior of  $U_x^{(\alpha\beta)}$  and  $U_y^{(\alpha\beta)}$  in an illustrative example. Consider  $m = n = 50$  with two sources, each 50-dimensional, generated independently from Gaussian distributions. Block-wise missingness is introduced by removing each source independently with probability 0.5 (regenerating if both are missing), yielding three observed patterns. The  $X$ -samples are drawn from  $\mathcal{N}_{100}(\mathbf{0}_{100}, \mathbf{I}_{100})$ , while the  $Y$ -samples follow one of four distributions: (a) the same null distribution; (b) a location shift  $\mathcal{N}_{100}(\mathbf{1}_{100}, \mathbf{I}_{100})$ ; (c) a scale shift  $\mathcal{N}_{100}(\mathbf{0}_{100}, 4\mathbf{I}_{100})$ ; or (d) a mixed alternative  $\mathcal{N}_{100}(0.5\mathbf{1}_{100}, 2\mathbf{I}_{100})$ .

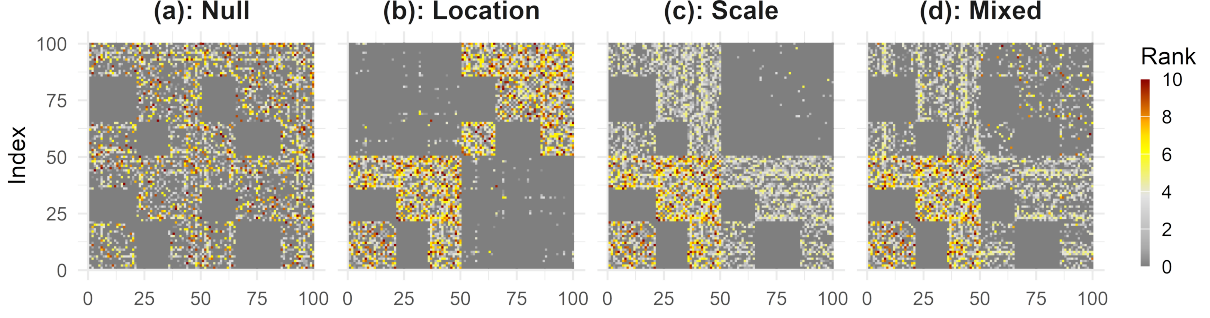


Figure 4: Heatmaps of pattern-wise rank matrices from 10-NNGs (three patterns).

Figure 4 shows heatmaps of the rank matrices. Under the location alternative, both  $U_x^{(\alpha\beta)}$  and  $U_y^{(\alpha\beta)}$  increase relative to their null values, whereas under the scale alternative, one tends to increase while the other decreases. For the mixed alternative, both  $U_x^{(\alpha\beta)}$  and  $U_y^{(\alpha\beta)}$  deviate from the null in different directions. These patterns motivate two complementary aggregation strategies: a vectorized form that is sensitive to localized deviations across patterns, and a low-dimensional aggregated form that captures overall distributional shifts.

Let  $\mathcal{I} = \{(\alpha, \beta) : 1 \leq \alpha \leq \beta \leq n_P, \mathcal{P}_\alpha \mathcal{P}_\beta^\top > 0\}$  be the set of valid pattern pairs. Define the vector  $V$  as the concatenation of

$$(U_x^{(\alpha\beta)} - \mu_x^{(\alpha\beta)}, U_y^{(\alpha\beta)} - \mu_y^{(\alpha\beta)}), \quad (\alpha, \beta) \in \mathcal{I},$$

so that  $V \in \mathbb{R}^{2|\mathcal{I}|}$ . Here  $\mu_x^{(\alpha\beta)} = \mathbb{E}(U_x^{(\alpha\beta)})$  and  $\mu_y^{(\alpha\beta)} = \mathbb{E}(U_y^{(\alpha\beta)})$ , with expectations taken under the pattern-wise permutation null distribution. The vectorized Block-wise RISE statistic (BRISÉ-v) is

$$T_v = V^\top \Sigma_v^{-1} V, \quad (3)$$

where  $\Sigma_v = \text{Cov}(V)$  is also evaluated under the pattern-wise permutation null distribution. By construction,  $T_v$  increases when any  $U_x^{(\alpha\beta)}$  or  $U_y^{(\alpha\beta)}$  deviates from its null expectation, making it sensitive to a broad range of alternatives.

Alternatively, consider the aggregated sums

$$U_x = \sum_{(\alpha, \beta) \in \mathcal{I}} U_x^{(\alpha\beta)} = \sum_{i=1}^m \sum_{j=1}^m R_{ij} \quad \text{and} \quad U_y = \sum_{(\alpha, \beta) \in \mathcal{I}} U_y^{(\alpha\beta)} = \sum_{i=m+1}^N \sum_{j=m+1}^N R_{ij},$$

which are equivalent to summing over all within-group ranks. The congregated Block-wise RISE statistic (BRISÉ-c) is

$$T_c = \bar{U}^\top \Sigma_c^{-1} \bar{U}, \quad (4)$$

where  $\bar{U} = (U_x - \mu_x, U_y - \mu_y)^\top$ ,  $\mu_x = \mathbb{E}(U_x)$ ,  $\mu_y = \mathbb{E}(U_y)$ , and  $\Sigma_c = \text{Cov}((U_x, U_y)^\top)$ .

BRISE-v is sensitive to heterogeneous local deviations but requires stable estimation of  $\Sigma_v$ , while BRISE-c is computationally more stable and better suited when  $n_P$  is large or sample sizes are limited.

**Remark 1.** *Other aggregation schemes are also possible. For example, weighted sums*

$$\tilde{U}_x = \sum_{(\alpha, \beta) \in \mathcal{I}} a_x^{(\alpha\beta)} U_x^{(\alpha\beta)}, \quad \tilde{U}_y = \sum_{(\alpha, \beta) \in \mathcal{I}} a_y^{(\alpha\beta)} U_y^{(\alpha\beta)}$$

*with prespecified weights could be substituted into (4), or one could consider maximum-type statistics such as  $\max_{(\alpha, \beta) \in \mathcal{I}, g \in \{X, Y\}} \{Z_g^{\alpha\beta}\}$  where  $Z_g^{\alpha\beta} = \frac{U_g^{(\alpha\beta)} - \mu_g^{(\alpha\beta)}}{\sigma_g^{(\alpha\beta)}}$  with  $\sigma_g^{(\alpha\beta)} = \text{Var}(U_g^{(\alpha\beta)})$ . Exploration of such alternatives is left for future work.*

**Remark 2.** *To avoid instability from extremely rare patterns, it is advisable to discard  $\mathcal{P}_\alpha$  with very small sizes, for instance those with  $\min\{m_\alpha, n_\alpha\} < n_{\text{thres}}$  or  $N_\alpha < p_{\text{thres}} \max_\beta N_\beta$ , using defaults such as  $n_{\text{thres}} = 2$  and  $p_{\text{thres}} = 0.1$ . The covariance matrices  $\Sigma_v$  and  $\Sigma_c$  should also be invertible. Simulations in Supplementary M show that both are typically stable, with  $\Sigma_c$  more robust in small samples. In rare cases of ill-conditioning, which occurs when some quantities  $U_g^{(\alpha\beta)}$ ,  $g \in \{x, y\}$ , are linearly dependent, a subset of these terms can be removed to ensure invertibility of the covariance matrix.*

## 3 Theoretical Properties

### 3.1 Finite-sample Properties

In this section, we provide explicit solution/formula to  $\Sigma_v$  and  $\Sigma_c$  under the null hypothesis, which is crucial to construct our proposed test statistics.

First, we define a collection of notations that are related to the rank matrix. Let  $\delta_{\alpha\beta} = \mathbb{1}(\alpha = \beta)$  be the Kronecker delta with the indicator function  $\mathbb{1}(\cdot)$ . We further define:

$$\begin{aligned} \bar{R}_{i\cdot}^{(\alpha\beta)} &= \frac{1}{N_\beta - \delta_{\alpha\beta}} \sum_{j=1}^{N_\beta} R_{ij}^{(\alpha\beta)}, & r_0^{(\alpha\beta)} &= \frac{1}{N_\alpha} \sum_{i=1}^{N_\alpha} \bar{R}_{i\cdot}^{(\alpha\beta)}, \\ (r_1^{(\alpha\beta\gamma)})^2 &= \frac{1}{N_\alpha} \sum_{i=1}^{N_\alpha} \bar{R}_{i\cdot}^{(\alpha\beta)} \bar{R}_{i\cdot}^{(\alpha\gamma)}, & (r_2^{(\alpha\beta)})^2 &= \frac{1}{N_\alpha(N_\beta - \delta_{\alpha\beta})} \sum_{i=1}^{N_\alpha} \sum_{j=1}^{N_\beta} (R_{ij}^{(\alpha\beta)})^2, \end{aligned}$$

$$V_1^{(\alpha\beta\gamma)} = (r_1^{(\alpha\beta\gamma)})^2 - r_0^{(\alpha\beta)} r_0^{(\alpha\gamma)}, \quad V_2^{(\alpha\beta)} = (r_2^{(\alpha\beta)})^2 - (r_0^{(\alpha\beta)})^2.$$

Here  $\bar{R}_i^{(\alpha\beta)}$  is the average rank per row of  $\mathbf{R}^{(\alpha\beta)}$ ;  $r_0^{(\alpha\beta)}$  is the mean of  $\bar{R}_i^{(\alpha\beta)}$ 's, which is also the average rank among  $\mathbf{R}^{(\alpha\beta)}$ ;  $(r_2^{(\alpha\beta)})^2$  and  $(r_1^{(\alpha\beta\gamma)})^2$  are the second-order moments;  $V_2^{(\alpha\beta)}$  and  $V_1^{(\alpha\beta\gamma)}$  are two types of variance term corresponding to  $r_2^{(\alpha\beta)}$  and  $r_1^{(\alpha\beta\gamma)}$ . We establish several useful properties of these quantities, valid for any symmetric matrix  $\mathbf{R}$  with zero diagonal; these properties simplify the calculation of  $\Sigma_v$  and  $\Sigma_c$ . Details are given in Supplementary C.

Let  $\mathcal{T}_x^{(\alpha,\beta)} = n_\alpha(m_\beta - 1 - \delta_{\alpha\beta})(N_\beta - \delta_{\alpha\beta})V_1^{(\alpha\beta\beta)}$ ,  $\mathcal{T}_y^{(\alpha,\beta)} = m_\alpha(n_\beta - 1 - \delta_{\alpha\beta})(N_\alpha - \delta_{\alpha\beta})V_1^{(\beta\alpha\alpha)}$ , and  $\mathcal{T}^{(\alpha,\beta)} = (N_\beta - \delta_{\alpha\beta})V_1^{(\alpha\beta\beta)}$ . Theorem 3 gives the explicit expression of basic quantities that are used to construct  $\Sigma_v$  and  $\Sigma_c$  in our test statistics.

**Theorem 3.** *Under the pattern-wise permutation null distribution, for  $1 \leq \alpha, \beta, \gamma \leq n_P$  and  $\beta \neq \gamma$ , with  $\min_{1 \leq \alpha \leq n_P} \{m_\alpha, n_\alpha\} \geq 2$ , we have*

$$\begin{aligned} \mu_x^{(\alpha\beta)} &= \mathbb{E}(U_x^{(\alpha\beta)}) = m_\alpha(m_\beta - \delta_{\alpha\beta})r_0^{(\alpha\beta)}, \quad \mu_y^{(\alpha\beta)} = \mathbb{E}(U_y^{(\alpha\beta)}) = n_\alpha(n_\beta - \delta_{\alpha\beta})r_0^{(\alpha\beta)}, \\ \text{Var}(U_x^{(\alpha\beta)}) &= \frac{(1 + \delta_{\alpha\beta})m_\alpha(m_\beta - \delta_{\alpha\beta})}{(N_\alpha - 1 - \delta_{\alpha\beta})(N_\beta - 1 - 2\delta_{\alpha\beta})} \left( n_\alpha(n_\beta - \delta_{\alpha\beta})V_2^{(\alpha\beta)} + \mathcal{T}_x^{(\alpha,\beta)} + \mathcal{T}_x^{(\beta,\alpha)} \right), \\ \text{Var}(U_y^{(\alpha\beta)}) &= \frac{(1 + \delta_{\alpha\beta})n_\alpha(n_\beta - \delta_{\alpha\beta})}{(N_\alpha - 1 - \delta_{\alpha\beta})(N_\beta - 1 - 2\delta_{\alpha\beta})} \left( m_\alpha(m_\beta - \delta_{\alpha\beta})V_2^{(\alpha\beta)} + \mathcal{T}_y^{(\alpha,\beta)} + \mathcal{T}_y^{(\beta,\alpha)} \right), \\ \text{Cov}(U_x^{(\alpha\beta)}, U_y^{(\alpha\beta)}) &= \frac{(1 + \delta_{\alpha\beta})m_\alpha n_\alpha(m_\beta - \delta_{\alpha\beta})(n_\beta - \delta_{\alpha\beta})}{(N_\alpha - 1 - \delta_{\alpha\beta})(N_\beta - 1 - 2\delta_{\alpha\beta})} \left( V_2^{(\alpha\beta)} - \mathcal{T}^{(\alpha,\beta)} - \mathcal{T}^{(\beta,\alpha)} \right), \\ \text{Cov}(U_x^{(\alpha\beta)}, U_x^{(\alpha\gamma)}) &= \frac{(1 + \delta_{\alpha\beta} + \delta_{\alpha\gamma})m_\alpha n_\alpha(m_\beta - \delta_{\alpha\beta})(m_\gamma - \delta_{\alpha\gamma})}{N_\alpha - 1 - \delta_{\alpha\beta} - \delta_{\alpha\gamma}} V_1^{(\alpha\beta\gamma)}, \\ \text{Cov}(U_y^{(\alpha\beta)}, U_y^{(\alpha\gamma)}) &= \frac{(1 + \delta_{\alpha\beta} + \delta_{\alpha\gamma})m_\alpha n_\alpha(n_\beta - \delta_{\alpha\beta})(n_\gamma - \delta_{\alpha\gamma})}{N_\alpha - 1 - \delta_{\alpha\beta} - \delta_{\alpha\gamma}} V_1^{(\alpha\beta\gamma)}, \\ \text{Cov}(U_x^{(\alpha\beta)}, U_y^{(\alpha\gamma)}) &= -\frac{(1 + \delta_{\alpha\beta} + \delta_{\alpha\gamma})m_\alpha n_\alpha(m_\beta - \delta_{\alpha\beta})(n_\gamma - \delta_{\alpha\gamma})}{N_\alpha - 1 - \delta_{\alpha\beta} - \delta_{\alpha\gamma}} V_1^{(\alpha\beta\gamma)}. \end{aligned}$$

*In cases other than above, the covariances are equal to 0.*

Using the result in Theorem 3, we can directly obtain the BRISE-v statistic. While for calculating BRISE-c, we can utilize the following relations:

$$\begin{aligned} \mu_x &= \mathbb{E}(U_x) = \sum_{(\alpha,\beta) \in \mathcal{I}} \mathbb{E}(U_x^{(\alpha\beta)}), \quad \mu_y = \mathbb{E}(U_y) = \sum_{(\alpha,\beta) \in \mathcal{I}} \mathbb{E}(U_y^{(\alpha\beta)}), \\ \text{Var}(U_x) &= \sum_{(\alpha,\beta) \in \mathcal{I}} \sum_{(\gamma,\omega) \in \mathcal{I}} \text{Cov}(U_x^{(\alpha\beta)}, U_x^{(\gamma\omega)}), \quad \text{Var}(U_y) = \sum_{(\alpha,\beta) \in \mathcal{I}} \sum_{(\gamma,\omega) \in \mathcal{I}} \text{Cov}(U_y^{(\alpha\beta)}, U_y^{(\gamma\omega)}), \end{aligned}$$

$$\text{Cov}(U_x, U_y) = \sum_{(\alpha, \beta) \in \mathcal{I}} \sum_{(\gamma, \omega) \in \mathcal{I}} \text{Cov}(U_x^{(\alpha\beta)}, U_y^{(\gamma\omega)}).$$

The proof of Theorem 3 is given in Supplementary D. Particularly, the moments  $\mathbb{E}(U_x^{(\alpha\beta)})$ ,  $\mathbb{E}(U_y^{(\alpha\beta)})$ ,  $\text{Var}(U_x^{(\alpha\beta)})$ ,  $\text{Var}(U_y^{(\alpha\beta)})$  and  $\text{Cov}(U_x^{(\alpha\beta)}, U_y^{(\alpha\beta)})$  will degenerate to the result in Theorem 1 of Zhou and Chen (2023) when  $\alpha = \beta$  (i.e., two patterns are the same); RISE can also be viewed as the special case with a single pattern in our proposed framework.

### 3.2 Asymptotic Properties

Exact  $p$ -value computation via full permutation is feasible for small samples but becomes intractable as sample size grows. To enable scalable inference, we derive the asymptotic distributions of the test statistics  $T_v$  and  $T_c$  under the null. We use the following asymptotic notations:  $a_n \prec b_n$  indicates  $a_n$  is dominated by  $b_n$ ;  $a_n \asymp b_n$  denotes boundedness above and below; and  $a_n \lesssim b_n$  denotes boundedness above. We adopt a standard regime where  $m_\alpha, n_\alpha \rightarrow \infty$ , with  $\lim_{N \rightarrow \infty} N_\alpha/N \in (0, 1)$  and  $m_\alpha/N_\alpha \rightarrow p_\alpha \in (0, 1)$  for all  $1 \leq \alpha \leq n_P$ .

To introduce our main result, we further define the following notations. For each pattern pair  $(\mathcal{Z}^{(\alpha)}, \mathcal{Z}^{(\beta)})$ , define the centered row sum  $\tilde{R}_{i\cdot}^{(\alpha\beta)} = \bar{R}_{i\cdot}^{(\alpha\beta)} - r_0^{(\alpha\beta)}$ . To capture the cross-pattern second-order dependence, we define

$$\mathbf{E}_\alpha = [\epsilon_{\alpha\beta\gamma}]_{\beta\gamma}, \text{ where } \epsilon_{\alpha\beta\gamma} = (r_1^{(\alpha\beta\gamma)})^2 - \frac{(r_1^{(\alpha\alpha\beta)})^2 (r_1^{(\alpha\alpha\gamma)})^2}{(r_1^{(\alpha\alpha\alpha)})^2} \text{ for } (\alpha, \beta), (\alpha, \gamma) \in \mathcal{I}, \beta \neq \alpha, \gamma \neq \alpha.$$

**Theorem 4** (Limiting distribution under the null hypothesis). *In the standard limit regime, for all  $(\alpha, \beta), (\beta, \gamma) \in \mathcal{I}$ , under Conditions*

$$\begin{aligned} (1) & r_1^{(\alpha\beta\beta)} \prec r_2^{(\alpha\beta)}; & (2) & \sum_{i=1}^{N_\alpha} \left( \sum_{j=1}^{N_\beta} (R_{ij}^{(\alpha\beta)})^2 \right)^2 \lesssim N_\alpha^2 N_\beta (r_2^{(\alpha\beta)})^4; \\ (3) & \sum_{i=1}^{N_\alpha} \left| \tilde{R}_{i\cdot}^{(\alpha\beta)} \right|^3 \prec (N_\alpha V_1^{(\alpha\beta\beta)})^{1.5}; & (4) & \sum_{i=1}^{N_\alpha} \left| \tilde{R}_{i\cdot}^{(\alpha\beta)} \right|^3 \prec N_\alpha r_2^{(\alpha\beta)} V_1^{(\alpha\beta\beta)}; \\ (5) & \left| \sum_{i=1}^{N_\alpha} \sum_{j=1}^{N_\beta} \sum_{\substack{l=1 \\ l \neq j}}^{N_\beta} R_{ij}^{(\alpha\beta)} R_{il}^{(\alpha\beta)} \tilde{R}_{j\cdot}^{(\beta\gamma)} \tilde{R}_{l\cdot}^{(\beta\gamma)} \right| \prec N_\alpha N_\beta^2 (r_2^{(\alpha\beta)})^2 V_1^{(\beta\gamma\gamma)}; \\ (6) & \sum_{i=1}^{N_\alpha} \sum_{j=1}^{N_\beta} \sum_{\substack{l=1 \\ l \neq i, j\delta_{\alpha\beta}}}^{N_\alpha} \sum_{\substack{s=1 \\ s \neq j, i\delta_{\alpha\beta}}}^{N_\beta} R_{ij}^{(\alpha\beta)} R_{lj}^{(\alpha\beta)} R_{is}^{(\alpha\beta)} R_{ls}^{(\alpha\beta)} \prec N_\alpha^2 N_\beta^2 (r_2^{(\alpha\beta)})^4. \end{aligned}$$

and (C1):  $\mathbf{E}_\alpha$  is positive definite, we have

$$T_v \xrightarrow{\mathcal{D}} \chi_a^2 \text{ and } T_c \xrightarrow{\mathcal{D}} \chi_2^2$$

under the pattern-wise permutation null distribution, where  $a = 2|\mathcal{I}|$  and  $\xrightarrow{\mathcal{D}}$  is convergence in distribution.

The proof of Theorem 4 is given in Supplementary E. The validity of Conditions (1)–(6) depends on the value of  $\alpha$ ,  $\beta$ , and  $\gamma$ . When  $\alpha = \beta = \gamma$ , the conditions degenerate to the conditions given in Theorem 4 in Zhou and Chen (2023), where it was argued that the conditions are mild and plausibly met in real data settings. When  $\alpha, \beta, \gamma$  are not all the same, Conditions (1), (2), (4), and (6) hold assuming that there are no nodes with a degree larger than  $Ck$  for some constant  $C$  in the pair-wise  $k$ -NNG defined in Section 2.2. To see this, let  $G^{(\alpha\beta)}$  be the  $k$ -NNG under pattern pair  $(\mathcal{Z}^{(\alpha)}, \mathcal{Z}^{(\beta)})$ , then we have  $k = \max_{\alpha\beta, ij} R_{ij}^{(\alpha\beta)}$ , and adopt the assumption that  $k \prec N$  for the graph-induced rank. With a slight abuse of notation, we use  $|\cdot|$  to denote the total weight of a graph. Usually we have  $r_0^{(\alpha\beta)} \asymp k|G^{(\alpha\beta)}|/N_\alpha N_\beta$  and  $(r_2^{(\alpha\beta)})^2 \asymp k^2|G^{(\alpha\beta)}|/N_\alpha N_\beta$  where  $|G^{(\alpha\beta)}| \asymp (N_\alpha + N_\beta)k/2$ . Thus, we have that Conditions (1), (2), (4), and (6) always hold as

$$\begin{aligned} (r_1^{(\alpha\beta\beta)})^2 &= \frac{1}{N_\alpha N_\beta^2} \sum_{i=1}^{N_\alpha} \left( \sum_{j=1}^{N_\beta} R_{ij}^{(\alpha\beta)} \right)^2 \asymp \frac{k^4}{N_\beta^2} \prec (r_2^{(\alpha\beta)})^2, \\ \sum_{i=1}^{N_\alpha} \left( \sum_{j=1}^{N_\beta} (R_{ij}^{(\alpha\beta)})^2 \right)^2 &\asymp N_\alpha (k^3)^2 \asymp N_\alpha (N_\alpha + N_\beta)^2 (r_2^{(\alpha\beta)})^4 \asymp N_\alpha^2 N_\beta (r_2^{(\alpha\beta)})^4, \\ \sum_{i=1}^{N_\alpha} |\tilde{R}_i^{(\alpha\beta)}|^3 &\leq \max_i |\tilde{R}_i^{(\alpha\beta)}| N_\alpha V_1^{(\alpha\beta\beta)} \lesssim \frac{k^2}{N_\alpha} N_\alpha V_1^{(\alpha\beta\beta)} \prec N_\alpha r_2^{(\alpha\beta)} V_1^{(\alpha\beta\beta)}, \\ \sum_{i=1}^{N_\alpha} \sum_{j=1}^{N_\beta} \sum_{l=1, l \neq i}^{N_\alpha} \sum_{s=1, s \neq j}^{N_\beta} R_{ij}^{(\alpha\beta)} R_{lj}^{(\alpha\beta)} R_{is}^{(\alpha\beta)} R_{ls}^{(\alpha\beta)} &\lesssim \sum_{i=1}^{N_\alpha} \sum_{j=1}^{N_\beta} R_{ij}^{(\alpha\beta)} \sum_{l=1}^{N_\alpha} R_{lj}^{(\alpha\beta)} \sum_{s=1}^{N_\beta} R_{is}^{(\alpha\beta)} R_{ls}^{(\alpha\beta)} \\ &\lesssim k \sum_{i=1}^{N_\alpha} \sum_{j=1}^{N_\beta} R_{ij}^{(\alpha\beta)} \sum_{l=1}^{N_\alpha} R_{lj}^{(\alpha\beta)} \sum_{s=1}^{N_\beta} R_{is}^{(\alpha\beta)} \asymp N_\alpha k^7 \asymp N_\alpha (N_\alpha + N_\beta)^2 k (r_2^{(\alpha\beta)})^4 \prec N_\alpha^2 N_\beta^2 (r_2^{(\alpha\beta)})^4. \end{aligned}$$

We further verify Conditions (3) and (5) by simulations. In our simulations, we calculate the ratio of the LHS to RHS of the inequality. Together with Condition (C1), simulation details and results are summarized in Supplementary N. The simulation results support that these conditions are easily satisfied.



Next, we discuss the consistency of BRISE. For the consistency under the standard limiting regime (see Theorem 5), Conditions (1)–(6) are not required. We consider  $G^{(\alpha\beta)}$  constructed using Euclidean distance. When  $k = O(1)$  and  $N_\alpha, N_\beta \rightarrow \infty$ , each edge in  $G^{(\alpha\beta)}$  exhibits asymptotically vanishing length, with connected nodes converging to arbitrarily close proximity in space (Henze and Penrose, 1999). This property arises because, in the limit, any point possesses sufficiently many neighbors within an arbitrarily small neighborhood to constitute its nearest neighbors. Under the choice of Euclidean distance, we have the following theorem.

**Theorem 5** (Consistency). *For two continuous multivariate distributions  $F_X$  and  $F_Y$  differing on a set of positive Lebesgue measure, employing the graph-induced rank with the  $k$ -NNG based on Euclidean distance, where  $k = O(1)$ , the power of both BRISE-v and BRISE-c at level  $\theta \in (0, 1)$  approaches 1 in the standard limiting regime.*

The proof of Theorem 5 is detailed in Supplementary F, following the methodologies of Schilling (1986) and Henze and Penrose (1999). This result may extend to alternative dissimilarity measures, provided they exhibit the same limiting behavior as described for  $G^{(\alpha\beta)}$ .

While Theorem 5 establishes the consistency of BRISE in the standard asymptotic settings, many modern applications, like genomics, neuroimaging, and text data, operate in the high-dimensional, low-sample-size (HDLSS) regime. In this context, classical asymptotic theory may fail due to the curse of dimensionality and degeneracy of distance metrics. The following result extends the consistency of BRISE to the HDLSS setting under mild moment and separation conditions.

**Theorem 6** (Consistency under HDLSS). *Assume that  $F_X$  and  $F_Y$  satisfy the following assumptions:*

(i) *There exist  $\sigma_{x,\alpha\beta}^2, \sigma_{y,\alpha\beta}^2 > 0$  and  $\nu_{\alpha\beta}^2 > 0$  such that for  $X^{(\alpha)} \in \mathcal{X}^{(\alpha)}$ ,  $X^{(\beta)} \in \mathcal{X}^{(\beta)}$ ,  $Y^{(\alpha)} \in \mathcal{Y}^{(\alpha)}$ , and  $Y^{(\beta)} \in \mathcal{Y}^{(\beta)}$  sampled independently from  $F_X$  and  $F_Y$ , for  $(\alpha, \beta) \in \mathcal{I}$ , the following limits hold:*

$$\frac{1}{d_{\alpha\beta}} \mathbb{E}(\rho(X^{(\alpha)}, \mathbb{E}X^{(\beta)})^2) \rightarrow \sigma_{x,\alpha\beta}^2, \frac{1}{d_{\alpha\beta}} \mathbb{E}(\rho(Y^{(\alpha)}, \mathbb{E}Y^{(\beta)})^2) \rightarrow \sigma_{y,\alpha\beta}^2, \frac{1}{d_{\alpha\beta}} \mathbb{E}(\rho(X^{(\alpha)}, \mathbb{E}Y^{(\beta)})^2) \rightarrow \nu_{\alpha\beta}^2,$$

*where  $d_{\alpha\beta}$  denotes the dimension of the overlapping sources for pattern pair  $(\mathcal{Z}_\alpha, \mathcal{Z}_\beta)$  and*

here  $\rho$  is the distance measure define in (1) with  $\rho_l$  being the squared Euclidean distance and  $\text{Norm}(x) = \sqrt{x}$ .

(ii) The fourth moments of the components of all observed sources are uniformly bounded.

(iii) Let  $Z_{iq}$  be the  $q$ th variable of a given observation  $Z_i$ . For  $(Z_{iq}, Z_{jq})_{Z_i \sim F_g, Z_j \sim F_{g'}}$  where  $g, g' \in \{X, Y\}$ , we assume the sequence  $\{(Z_{iq}, Z_{jq}), q \geq 1\}$  is  $\rho'$ -mixing, i.e.,

$$\sup_{1 \leq q < q' < \infty, |q - q'| > r} |\text{corr}\{(Z_{iq} - Z_{jq})^2, (Z_{iq'} - Z_{jq'})^2\}| \leq \rho'(r),$$

with  $\rho'(r) \rightarrow 0$  as  $r \rightarrow \infty$ .

For any fixed significance level  $\theta \in (0, 1)$ , we have

$$\lim_{d \rightarrow \infty} P(T_v > \chi_a^2(1 - \theta)) = 1 \quad \text{and} \quad \lim_{d \rightarrow \infty} P(T_c > \chi_2^2(1 - \theta)) = 1,$$

where the probability here is under the alternative hypothesis if the alternative hypothesis satisfies the following conditions:

1.  $k < \min_{1 \leq \alpha \leq n_P} \{n_\alpha, m_\alpha\}$ ,  $\lim_{d \rightarrow \infty} d_{\alpha\beta}/d \in (0, 1)$  for all  $1 \leq \alpha \leq \beta \leq n_P$ ;
2. There exists at least one  $(\alpha, \beta)$  such that either  $\sigma_{x,\alpha\beta}^2 \neq \sigma_{y,\alpha\beta}^2$  or  $\nu_{\alpha\beta}^2 > 0$ ;
3. The largest eigenvalue of the covariance matrix  $\Sigma_v$  satisfies  $\lambda_+[\Sigma_v] = O(N^{2-b})$  for some  $b > 0$ ,  $N \geq C_{b,\theta}$  for a constant  $C_{b,\theta} > 0$  only depending on  $b, \theta$ .

Assumptions (i)-(iii) of Theorem 6 are extended from Biswas and Ghosh (2014), with the proof of the theorem provided in Supplementary G. Here we only consider the overlapping Euclidean distance case of the dissimilarity measure given in (1). If using other measuring methods, our proposed tests may still be consistent under HDLSS as long as they have similar limiting constraints under suitable conditions.

## 4 Simulation Studies

We conduct simulation studies to evaluate the empirical type-I error and power of BRISE. We consider both BRISE-c and BRISE-v with Euclidean distance in (1) and  $k = 10$  for constructing the  $k$ -NNG, following the recommendation of Zhou and Chen (2023). We also examine the sensitivity of our methods to the choice of  $k$  (see additional results reported

in Supplementary O). The findings indicate that the performance of BRISE is stable with respect to  $k$ , as long as  $k$  is not chosen too small. For both variants,  $p$ -values are obtained using their asymptotic null distributions.

We compare our methods with five baselines: MMD-Miss, RISE with  $k$ -NNG, the standard MMD test (Gretton et al., 2012), Ball Divergence (BD) (Pan et al., 2018), and Measure Transportation (MT) (Deb and Sen, 2021). Among these, only MMD-Miss can be directly applied to incomplete data; the others are implemented using complete-case analysis. The  $p$ -values of MMD-Miss, MMD, MT, and BD are obtained using 1000 permutations, while RISE uses its asymptotic null distribution for  $p$ -value calculation. For RISE, we set  $k = 10$ , and for the other baselines, we adopt their default hyperparameters. To further examine the advantage of the proposed pattern-wise permutation procedure in type-I error control, we also include a variant of BRISE-c that differs only in the permutation scheme, using standard instead of pattern-wise permutation, denoted as BRISE-c(sp). According to Theorem 1, this variant may fail when the marginal pattern probabilities differ between groups.

Data are generated as follows. For each observation, every source  $Z^{(l)} \in \mathbb{R}^{d_l}$  is generated and observed independently with probability  $p_{g,l}$  for  $g \in X, Y$ ; observations with all sources missing are discarded. To reflect a variety of realistic scenarios, we simulate a wide range of null and alternative distributions in moderate to high-dimensional settings. These include multivariate Gaussian, log-normal, and  $t_5$  distributions, covering both light-tailed and heavy-tailed behaviors. The alternative hypotheses encompass differences in location, scale, and their combinations.

We further define  $d = \sum_{l=1}^L d_l$ . For simplicity, we assume that all sources within the same group  $g \in \{X, Y\}$  share a common sampling rate  $p_g$ , and that the  $d_l$ 's are identical across sources. Specifically, we consider the following source distributions:

(I) **Multivariate Gaussian.**  $(X^{(1)}, \dots, X^{(L)}) \sim \mathcal{N}_d(\mathbf{0}_d, \Sigma_X)$ , where  $\Sigma_{X,ij} = 0.6^{|i-j|}$ .  
 $(Y^{(1)}, \dots, Y^{(L)}) \sim F_Y(\cdot)$ , where  $F_Y(\cdot)$  is:

- a. *Location:*  $\mathcal{N}_d(\boldsymbol{\mu}, \Sigma_X)$ , where  $\boldsymbol{\mu} = 0.4 \log d \cdot \boldsymbol{\mu}' / \|\boldsymbol{\mu}'\|_2$  and  $\boldsymbol{\mu}' \sim \mathcal{N}_d(0_d, I_d)$ .
- b. *Scale:*  $\mathcal{N}_d(\mathbf{0}_d, \sigma^2 \Sigma_X)$ , with  $\sigma = 1 + 0.12 \log d / \sqrt{d}$ .
- c. *Location and scale:*  $\mathcal{N}_d(\boldsymbol{\mu}, \Sigma_Y)$ , where  $\boldsymbol{\mu} = 0.1 \log d \cdot \boldsymbol{\mu}' / \|\boldsymbol{\mu}'\|_2$ ,  $\boldsymbol{\mu}' \sim \mathcal{N}_d(0_d, I_d)$ , and  $\Sigma_{Y,ij} = 0.3^{|i-j|}$ .

(II) **Multivariate Log-Normal.**  $(X^{(1)}, \dots, X^{(L)}) \sim \exp(\mathcal{N}_d(\mathbf{0}_d, \Sigma_X))$ , with  $\Sigma_{X,ij} = 0.6^{|i-j|}$ .  
 $(Y^{(1)}, \dots, Y^{(L)}) \sim F_Y(\cdot)$ , where  $F_Y(\cdot)$  is:

- a. *Location:*  $\exp(\mathcal{N}_d(\boldsymbol{\mu}, \Sigma_X))$ , where  $\mu_j = (-1)^j \cdot 2 \log d / \sqrt{d}$  for  $j = 1, \dots, \lfloor 0.05d \rfloor$ , and  $\mu_j = 0$  otherwise.
- b. *Scale:*  $\exp(\mathcal{N}_d(\mathbf{0}_d, \sigma^2 \Sigma_X))$ , with  $\sigma = 1 + 0.15 \log d / \sqrt{d}$ .
- c. *Location and scale:*  $\exp(\mathcal{N}_d(\mu \mathbf{1}_d, \sigma \Sigma_X))$ , where  $\mu = 0.25 \log d / \sqrt{d}$  and  $\sigma = 1 + 0.1 \cdot (50/d)^{0.25}$ .

(III) **Multivariate Student- $t$ .**  $(X^{(1)}, \dots, X^{(L)}) \sim t_5(\mathbf{0}_d, \Sigma_X)$ , where  $\Sigma_{X,ij} = 0.6^{|i-j|}$ .  
 $(Y^{(1)}, \dots, Y^{(L)}) \sim F_Y(\cdot)$ , where  $F_Y(\cdot)$  is:

- a. *Location:*  $t_5(\boldsymbol{\mu}, \Sigma_X)$ , where  $\mu_j = (-1)^j \cdot 2 \log d / \sqrt{d}$  for  $j = 1, \dots, \lfloor 0.05d \rfloor$ , and  $\mu_j = 0$  otherwise.
- b. *Scale:*  $t_5(\mathbf{0}_d, \Sigma_Y)$ , where  $\Sigma_{Y,ij} = 0.75 \cdot 0.3^{|i-j|}$ .
- c. *Location and scale:*  $t_5(\mu \mathbf{1}_d, \Sigma_Y)$ , with  $\mu = 0.4 \log d / \sqrt{d}$  and  $\Sigma_{Y,ij} = 0.8^{|i-j|}$ .

We set the default setting as  $m = n = 100$ ,  $L = 2$ ,  $p_X = p_Y = 0.5$ , and  $d \in \{200, 500, 1000\}$ . To validate the performance of tests under diverse scenarios, we also include additional experiments on power of tests with imbalanced sample sizes ( $m = 200, n = 100$ ), increased numbers of sources ( $L = 3$ ), varied sampling rates ( $p_X = p_Y \in \{0.2, 0.8\}$ ) and imbalanced sampling rates ( $p_X = 0.5, p_Y = 0.8$ ) in Supplementary O. We repeat 1000 times for simulations of empirical sizes and 100 times for simulations of power of tests.

At significance level  $\theta = 0.05$ , the empirical sizes under both balanced and imbalanced sampling rates under different groups are reported in Table 1. As shown in the table, when the sampling rates are balanced, all methods have acceptable type-I error. But when the sampling rates are imbalanced, BRISE-c, BRISE-v, MMD-Miss and methods using complete cases still control type-I error well, while BRISE-c(sp) fails to control the type I error. This highlights the advantage of our methods on considering block-wise missingness mechanism.

The estimated powers of the tests under the default setting are provided in Table 2. Across all dimensions, the BRISE family consistently achieves superior statistical power compared to the baselines. In particular, BRISE-c demonstrates the most robust performance, maintaining high power across a broad range of distributional differences.

Table 1: Empirical sizes of the tests at significance level  $\theta = 0.05$ , for  $m = n = 100$ ,  $L = 2$ , repeated 1000 times. Here we use *italic* type to denote values way higher than 0.05.

$d$	200	500	1000	200	500	1000	200	500	1000
$p_X = p_Y = 0.5$	Setting I			Setting II			Setting III		
BRISE-c	0.035	0.041	0.065	0.039	0.049	0.061	0.056	0.047	0.043
BRISE-v	0.031	0.045	0.049	0.055	0.050	0.047	0.056	0.051	0.043
MMD-Miss	0.000	0.000	0.000	0.000	0.000	0.000	0.000	0.000	0.000
RISE	0.041	0.040	0.060	0.048	0.042	0.055	0.054	0.057	0.039
MMD	0.000	0.000	0.000	0.002	0.000	0.000	0.005	0.004	0.002
BD	0.045	0.040	0.050	0.052	0.043	0.057	0.052	0.041	0.039
MT	0.044	0.043	0.057	0.042	0.040	0.061	0.047	0.035	0.039
BRISE-c(sp)	0.034	0.048	0.064	0.045	0.051	0.058	0.045	0.048	0.046
$p_X = 0.5, p_Y = 0.8$	Setting I			Setting II			Setting III		
BRISE-c	0.037	0.047	0.064	0.040	0.044	0.046	0.043	0.040	0.049
BRISE-v	0.040	0.042	0.054	0.044	0.042	0.045	0.045	0.045	0.048
MMD-Miss	0.000	0.000	0.000	0.000	0.000	0.000	0.000	0.000	0.000
RISE	0.045	0.040	0.061	0.048	0.055	0.043	0.050	0.048	0.050
MMD	0.004	0.000	0.000	0.004	0.000	0.000	0.008	0.009	0.008
BD	0.062	0.047	0.050	0.058	0.054	0.047	0.044	0.048	0.043
MT	0.048	0.044	0.059	0.047	0.050	0.051	0.057	0.045	0.039
BRISE-c(sp)	<i>0.193</i>	<i>0.200</i>	<i>0.213</i>	<i>0.281</i>	<i>0.336</i>	<i>0.391</i>	<i>0.319</i>	<i>0.375</i>	<i>0.451</i>

Under the multivariate Gaussian distribution (Setting I), BRISE-c demonstrates consistently superior performance across all three subsettings, achieving the highest power for location, scale, and mixed alternatives. BRISE-v follows closely, showing strong power in most subsettings. In contrast, RISE and BD exhibit moderate power in scale settings but perform weakly in location and mixed cases. MMD shows limited power, with some effectiveness for location alternatives at lower dimensions ( $d = 200$ ). MT also exhibits limited power across all subsettings, with slightly better performance for mixed alternatives at higher dimensions ( $d = 1000$ ). MMD-Miss fails to show any power across all subsettings, as it is not designed for data with block-wise missingness in high dimensions.

For the multivariate log-normal distribution (Setting II), BRISE-v performs strongly in detecting location differences across all dimensions. BRISE-c dominates in scale and mixed subsettings, achieving the highest power. BD is competitive in scale and mixed settings,

Table 2: Estimated powers at significance level  $\theta = 0.05$ , for  $m = n = 100$ ,  $L = 2$  and  $p_X = p_Y = 0.5$ . Under the multivariate Gaussian I: a. Location, b. Scale, and c. Mixed; the multivariate log-normal II: a. Location, b. Scale, and c. Mixed; and the multivariate  $t_5$  III: a. Location, b. Scale, and c. Mixed. Top-1, Top-2 powers are in **bold** and underlined, respectively.

$d$	200	500	1000	200	500	1000	200	500	1000
Method	Setting I-a			Setting I-b			Setting I-c		
BRISE-c	<b>84</b>	<b>67</b>	<b>57</b>	<b>82</b>	<b>90</b>	<b>97</b>	<b>96</b>	<b>97</b>	<b>87</b>
BRISE-v	<u>65</u>	<u>43</u>	<u>33</u>	53	68	74	<u>75</u>	<u>75</u>	<u>69</u>
MMD-Miss	0	0	0	0	0	0	0	0	0
RISE	34	23	21	55	60	69	29	24	20
MMD	14	0	0	0	0	0	0	0	0
BD	15	9	8	<u>65</u>	<u>77</u>	<u>85</u>	10	4	12
MT	7	6	2	2	4	5	7	5	14
Method	Setting II-a			Setting II-b			Setting II-c		
BRISE-c	<b>78</b>	<u>49</u>	<u>38</u>	<b>53</b>	<b>38</b>	<u>57</u>	<b>86</b>	<b>85</b>	<b>89</b>
BRISE-v	<u>77</u>	<b>59</b>	<b>48</b>	31	20	25	63	53	59
MMD-Miss	0	0	0	0	0	0	0	0	0
RISE	29	19	14	20	15	25	45	44	39
MMD	10	0	0	0	0	1	27	5	0
BD	9	5	7	<u>41</u>	<u>35</u>	<b>59</b>	<u>68</u>	<u>67</u>	<u>83</u>
MT	8	12	18	12	11	10	51	35	43
Method	Setting III-a			Setting III-b			Setting III-c		
BRISE-c	<u>94</u>	<u>80</u>	<u>58</u>	<b>85</b>	<b>75</b>	<b>64</b>	<b>96</b>	<b>83</b>	<b>69</b>
BRISE-v	<b>98</b>	<b>91</b>	<b>81</b>	<u>74</u>	<u>64</u>	<u>51</u>	<u>91</u>	<u>73</u>	<u>58</u>
MMD-Miss	0	0	0	0	0	0	0	0	0
RISE	55	33	19	39	35	22	42	28	22
MMD	7	1	0	7	12	9	12	1	0
BD	4	6	4	42	41	37	4	6	3
MT	13	11	9	8	11	8	41	24	27

especially at higher dimensions, but is outperformed by BRISE-c. RISE, MMD, and MT exhibit moderate power, with RISE and MT performing well for mixed alternatives across all dimensions. MMD-Miss shows no power in this block-wise missingness scenario.

With the heavy-tailed multivariate  $t_5$  distribution (Setting III), BRISE-v achieves the

highest power for location shifts. BRISE-c excels in scale and mixed alternatives, outperforming other methods. RISE shows moderate power across all alternatives. BD exhibits moderate power in the scale setting but low power otherwise. MT shows moderate power in the mixed setting but low power in other alternatives.

Under Setting I, we further study the trend of statistical power of all the methods when  $p_X$  and  $p_Y$  vary simultaneously ( $p_X = p_Y \in \{0, 0.1, \dots, 0.9, 1\}$ ); see Figure 5. BRISE-c consistently achieves high power across most dimensions and probability values, while BRISE-v also exhibits reasonably high powers; both BRISE variants are robust to variations in sampling rates, with only minor power reduction as sampling rates decrease. In contrast, other methods (MMD-Miss, RISE, MMD, BD, MT) suffer significant power loss under decreasing sampling rates or fail to perform effectively at nearly all sampling rates. Specifically, when sampling rates are high, we observe that MMD performs best under Setting I-a; BD is very powerful under Setting I-b, the scale alternative; while RISE precedes under Setting I-c, the mixed alternative. However, these methods suffer from reduced sample size at low sampling rates, underscoring the robustness of BRISE. MT and MMD-Miss show limited effectiveness across most alternatives in Setting I. Critically, BRISE’s resilience to missingness is consistently observed across other experimental settings beyond Setting I (see Supplementary O), underscoring its general reliability.

In addition, we conduct simulations under other hyperparameter scenarios, with the corresponding results presented in Supplementary O. Specifically, for scenarios with imbalanced sample sizes, they show similar phenomena to the default setting; for scenarios with different sampling probabilities, including both lower and higher cases, we observe that BRISE-family methods are more powerful at lower sampling rates compared to other methods; we also examine scenarios where  $p_X \neq p_Y$ , and the simulation power still exhibits similar behaviors as in the default case. Furthermore, we explore settings with an increased number of sources, specifically  $L = 3$ . In this scenario, the power of all BRISE methods remains at the same level or degrades only slightly compared to the two-source case, while other methods using complete-case analysis suffer significant power loss due to smaller sample sizes.

In summary, the simulation results provide strong empirical support for the effectiveness of the BRISE family of tests. Each variant demonstrates a unique strength for certain alternatives. Collectively, utilizing the BPET framework, BRISE significantly outperforms

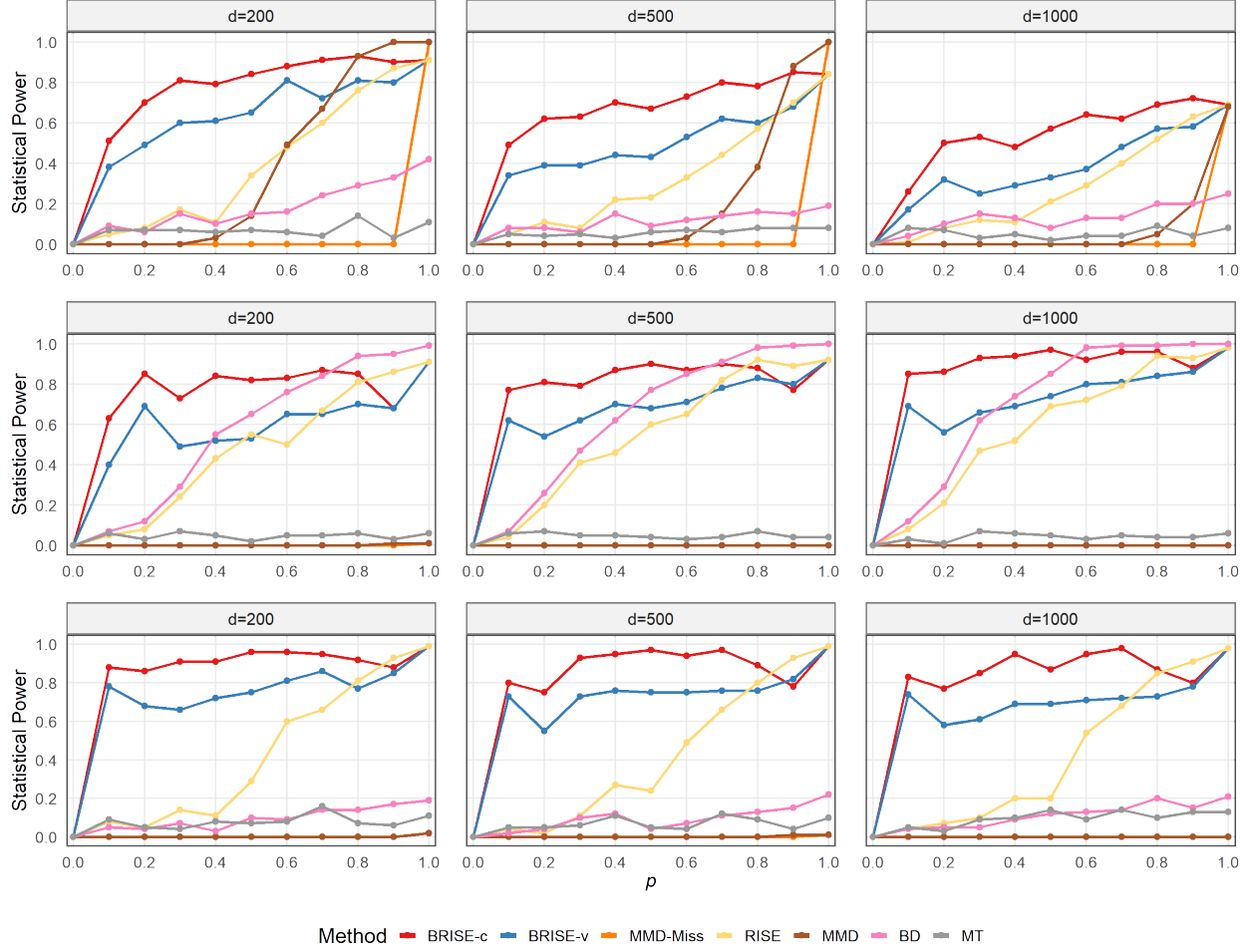


Figure 5: Trend of estimated powers vs.  $p$  at significance level  $\theta = 0.05$ , for  $m = n = 100$ ,  $L = 2$ ,  $p_X = p_Y = p$  and  $d \in \{200, 500, 1000\}$ . Top: Setting I-a; Middle: Setting I-b; Bottom: Setting I-c.

traditional tests, making it well-suited for modern high-dimensional two-sample testing problems.

## 5 Real Data Analysis

### 5.1 Sepsis Identification Using Multi-source Biomarkers

We now illustrate the utility of the BRISE using a sepsis study. Sepsis is a major public health concern in the United States, characterized by the body's pathologic response to infection,



which can lead to tissue damage, organ failure, and death (Singer et al., 2016). Identifying biomarkers that can provide early warning signs and enable timely, targeted interventions is therefore crucial for the treatment of sepsis. The goal of this study is to examine potential differences in age, sex, race, APACHE II, absolute neutrophil count (ANC), absolute lymphocyte count (ALC), monocyte distribution width (MDW), and other biomarkers among septic patients and patients who were considered critically ill without sepsis (CINS).

Most single studies involving these biomarkers have relatively small sample sizes or focus on patients who present to the emergency department with community-acquired sepsis (Agnello et al., 2021). In contrast, this study evaluates whether biomarker distributions differ between septic patients and CINS in the context of purely hospital-acquired sepsis as observed in surgical and trauma ICUs. This task is particularly challenging and important: patients admitted to surgical/trauma ICUs often experience concomitant inflammation due to surgical or traumatic injury (clinically difficult to distinguish from sepsis) and are at heightened risk of sepsis due to invasive procedures, indwelling devices (e.g., catheters, ventilators), and compromised immune state from prolonged hospitalization or underlying health conditions (Mas-Celis et al., 2021; Cohen et al., 2023).

To investigate this question, we combined data from three prospective observational studies of hospitalized patients admitted to a surgical ICU at a quaternary-care academic health science center. Two studies were conducted by the UF Sepsis and Critical Illness Research Center (SCIRC) and are registered on clinicaltrials.gov (NCT04414189, NCT05110937) (Brakenridge et al., 2021). The third study involved subjects enrolled at Shands-UF Hospital as part of an NIGMS-funded consortium (Barrios et al., 2024). A key challenge in this analysis is the presence of block-wise missingness arising from differences in study protocols. Specifically, in two studies, biomarkers were measured on Days 1 and 4, while in the third study they were measured on Day 2. No single study collected biomarkers on all days, leading to a block-missing pattern in the combined dataset.

The final dataset includes 56 septic patients ( $X$ ) and 74 non-septic patients ( $Y$ ). Figure 6 provides a heatmap visualization of the biomarker data, with gray indicating missing values.

Table 3 reports the  $p$ -values obtained from our method and benchmark approaches. Both BRISE variants detect highly significant differences between septic and non-septic patients. In contrast, MMD-Miss fails to reject the null hypothesis, reflecting its conservative behavior,

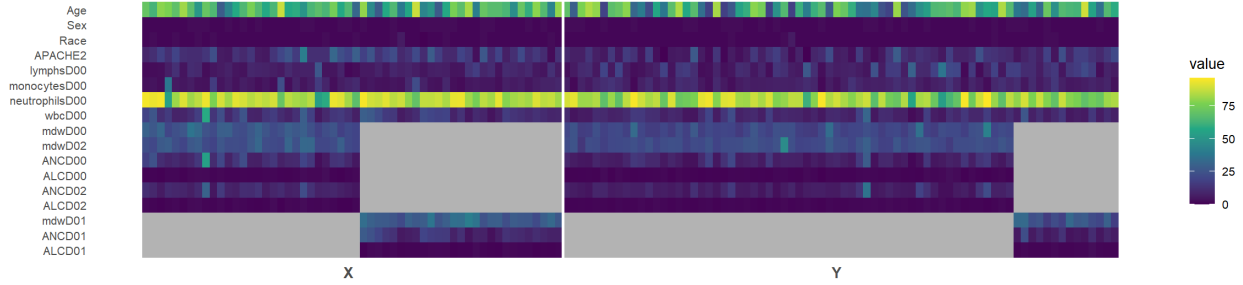


Figure 6: Heatmap visualization of sepsis biomarker data. Gray indicates missing values.

as it was not designed for this type of setting. Complete-case (CC) analysis is not applicable here, as no complete cases are available. These results underscore the superior performance and robustness of BRISE in real-world biomedical studies with block-wise missingness.

Table 3: The  $p$ -values of the tests for the sepsis data. Significant values are shown in **bold**.

Method	BRISE-c	BRISE-v	MMD-Miss	CC Analysis
Sepsis/CINS	<b>5.38e-14</b>	<b>3.89e-15</b>	1	n.a.

## 5.2 Multi-modal Differentiation of Alzheimer’s Disease

A critical real-world application of multi-modal statistical analysis is in distinguishing between cognitive health states based on medical data. In particular, Alzheimer’s Disease (AD) and cognitively normal (CN) conditions often exhibit subtle but detectable differences across biomarkers, imaging features, and metabolic indicators. Accurate identification of these differences is crucial for early diagnosis, targeted intervention, and a better understanding of disease mechanisms.

To evaluate the practical effectiveness of our methods, we apply them to the Alzheimer’s Disease Neuroimaging Initiative (ADNI) dataset (Mueller et al., 2005a). Each ADNI participant is uniquely identified by a Participant Roster ID (RID). Following the approach of Balsis et al. (2015), we define diagnostic groups using Mini-Mental State Examination (MMSE) scores (Folstein et al., 1975): individuals with MMSE scores greater than 24 and up to 30 are classified as CN, while those with scores of 24 or below are classified as AD. For individuals with multiple MMSE measurements, we use the average score for consistency.

Our analysis integrates three modalities: Magnetic Resonance Imaging (MRI), Positron Emission Tomography (PET), and biospecimen data. MRI and PET image data are processed into numeric variables by the Center for Imaging of Neurodegenerative Diseases at the University of California, San Francisco, and the Jagust Lab at the University of California, Berkeley, respectively. The biospecimen data, analyzed by the Proteomics and Metabolomics Shared Resource at Duke University, provide serum measurements of selected metabolites, including biomarkers such as carnitine and decanoylcarnitine. All data are available through the Analysis Ready Cohort (ARC) Builder<sup>1</sup>.

We merge the three modalities using RID after removing cases with random missingness. The proposed methods are then evaluated on two datasets: (i) a balanced subset (Sub) consisting of 200 randomly selected individuals from each group (AD and CN), and (ii) the full dataset (Full) comprising all available samples, including 2,047 CN and 507 AD subjects. Each method is assessed using both permutation-based (P) inference (1000 permutations) and asymptotic (A) null approximations when available.

Table 4 reports the resulting  $p$ -values. Both BRISE variants achieve highly significant results across all datasets and inference types, demonstrating superior statistical power even under substantial block-wise missingness. By contrast, RISE, MMD, and BD yield significant results only on the full dataset and fail to reject the null hypothesis in the balanced subset. MMD-Miss produces  $p$ -values equal to 1 in all settings, likely due to its inability to leverage cross-pattern structure. MT fails in both datasets, further illustrating its limited robustness for incomplete multi-modal data. These findings align with our simulation studies and highlight the practical applicability of BRISE for detecting group differences in high-dimensional, block-wise incomplete settings.

Table 4: The  $p$ -values of the tests for the ADNI data. Significant values are shown in **bold**.

Method	BRISE-c	BRISE-v	MMD-Miss	RISE	MMD	BD	MT
Sub(P)	<b>0</b>	<b>0</b>	1	0.081	0.195	0.159	0.335
Sub(A)	<b>3.56e-13</b>	<b>7.96e-11</b>	1	0.074	-	-	-
Full(P)	<b>0</b>	<b>0</b>	1	<b>0.003</b>	<b>0.031</b>	<b>0.017</b>	0.142
Full(A)	<b>0</b>	<b>0</b>	1	<b>3.22e-05</b>	-	-	-

<sup>1</sup>[https://ida.loni.usc.edu/explore/jsp/search\\_v2/search.jsp?project=ADNI](https://ida.loni.usc.edu/explore/jsp/search_v2/search.jsp?project=ADNI)

## 6 Discussion and Conclusion

In this work, we propose a general framework, called BPET, for two-sample testing under block-wise missingness without requiring imputation or deletion of observations, enabling reliable inference with incomplete datasets. Further, we incorporate the rank-based RISE test within the proposed BPET framework to account for possible multiple modalities. We established the finite-sample properties, validity, and consistency of the proposed methods. Their effectiveness was demonstrated through both extensive simulations and two real-world applications, and the BRISE implementation exhibited strong empirical performance. Although developed for two-sample testing, BPET can be readily extended to other inferential tasks such as independence testing, clustering, and change-point detection in the presence of block-wise missingness.

As a general framework, we emphasize that BPET is not limited to graph/rank-based methods; a broad class of two-sample test procedures can be applied within the BPET framework. For example, by computing pattern-wise dissimilarities or kernel metrics (Section 2.1), both kernel-based, and distance-based methods can be incorporated into BPET. Beyond the  $k$ -NNG, other similarity graphs such as  $k$ -MST (Friedman and Rafsky, 1979) and  $k$ -MDP (Rosenbaum, 2005) may also be used. These approaches follow the same principle: partition the data into missingness patterns, perform pattern-specific computations, and aggregate the results into a global test statistic. The finite-sample properties established in Section 3.1 can be extended, provided the method produces a symmetric similarity matrix such as  $\mathbf{R}$ .

In multi-modal data, it is common that samples from different patterns have non-overlapping variables (or modalities). In the main text, we proposed the zero-filling strategy in Section 2.1; one may also adopt alternative measures, such as rank-based distances (Supplementary L) or embedding all sources into a latent subspace (e.g., via partial multi-view clustering (Li et al., 2014; Zhao et al., 2016; Wang et al., 2018; Feng et al., 2024)) before computing distances on the aligned projections. An interesting observation from our simulation is that the proposed method leveraging the zero-filling strategy consistently outperforms other dissimilarity measures. This raises a future research question: whether information from samples without shared or overlapping sources/modalities is important, and if so, how to efficiently leverage it. Our work is among the first to explore these important questions.

## References

- Agnello, L., B. L. Sasso, R. V. Giglio, G. Bivona, C. M. Gambino, A. Cortegiani, A. M. Ciaccio, M. Vidali, and M. Ciaccio (2021). Monocyte distribution width as a biomarker of sepsis in the intensive care unit: a pilot study. *Annals of Clinical Biochemistry* 58(1), 70–72.
- Aleksić, D. G. and B. Milošević (2025). Two-sample testing with missing data via energy distance: Weighting and imputation approaches. *arXiv preprint arXiv:2508.11421*.
- Balsis, S., J. Bengt, D. Lowe, L. Geraci, R. Doody, and f. ADNI (2015, 11). How do scores on the adas-cog, mmse, and cdr-sob correspond? *The Clinical Neuropsychologist* 29.
- Barrios, E. L., M. B. Mazer, P. W. McGonagill, C. B. Bergmann, M. D. Goodman, R. W. Gould, M. Rao, V. E. Polcz, R. J. Davis, D. E. Del Toro, et al. (2024). Adverse outcomes and an immunosuppressed endotype in septic patients with reduced ifn- $\gamma$  elispot. *JCI Insight* 9(2), e175785.
- Biswas, M. and A. K. Ghosh (2014). A nonparametric two-sample test applicable to high dimensional data. *Journal of Multivariate Analysis* 123, 160–171.
- Borah, S., V. Chandola, and V. Kumar (2008). Similarity measures for categorical data: A comparative evaluation. In *Proceedings of the 2008 SIAM International Conference on Data Mining*, pp. 243–254. SIAM.
- Brakenridge, S. C., P. Starostik, G. Ghita, U. Midic, D. Darden, B. Fenner, J. Wacker, P. A. Efron, O. Liesenfeld, T. E. Sweeney, et al. (2021). A transcriptomic severity metric that predicts clinical outcomes in critically ill surgical sepsis patients. *Critical Care Explorations* 3(10), e0554.
- Chen, H., X. Chen, and Y. Su (2018). A weighted edge-count two-sample test for multivariate and object data. *Journal of the American Statistical Association* 113(523), 1146–1155.
- Chen, H. and J. H. Friedman (2017). A new graph-based two-sample test for multivariate and object data. *Journal of the American Statistical Association* 112(517), 397–409.
- Chen, H. and N. R. Zhang (2013). Graph-based tests for two-sample comparisons of categorical data. *Statistica Sinica*, 1479–1503.
- Cohen, N. S., J. M. Bock, and A. K. May (2023). Sepsis and postoperative surgical site infections. *Surgery* 174(2), 403–405.

- Deb, N. and B. Sen (2021, 05). Multivariate rank-based distribution-free nonparametric testing using measure transportation. *Journal of the American Statistical Association* 118, 1–45.
- Eric, M., F. Bach, and Z. Harchaoui (2007). Testing for homogeneity with kernel fisher discriminant analysis. *Advances in Neural Information Processing Systems* 20.
- Feng, W., G. Sheng, Q. Wang, Q. Gao, Z. Tao, and B. Dong (2024). Partial multi-view clustering via self-supervised network. In *Proceedings of the AAAI Conference on Artificial Intelligence*, Volume 38, pp. 11988–11995.
- Folstein, M. F., S. E. Folstein, and P. R. McHugh (1975). “mini-mental state”: a practical method for grading the cognitive state of patients for the clinician. *Journal of Psychiatric Research* 12(3), 189–198.
- Friedman, J. H. and L. C. Rafsky (1979). Multivariate generalizations of the wald-wolfowitz and smirnov two-sample tests. *The Annals of Statistics* 7(4), 697–717.
- Gretton, A., K. Borgwardt, M. Rasch, B. Schölkopf, and A. Smola (2006). A kernel method for the two-sample-problem. In B. Schölkopf, J. Platt, and T. Hoffman (Eds.), *Advances in Neural Information Processing Systems*, Volume 19. MIT Press.
- Gretton, A., K. Borgwardt, M. Rasch, B. Schölkopf, and A. Smola (2012, 03). A kernel two-sample test. *The Journal of Machine Learning Research* 13, 723–773.
- Gretton, A., K. Fukumizu, Z. Harchaoui, and B. K. Sriperumbudur (2009). A fast, consistent kernel two-sample test. *Advances in Neural Information Processing Systems* 22.
- Hammond, D. K., Y. Gur, and C. R. Johnson (2013). Graph diffusion distance: A difference measure for weighted graphs based on the graph laplacian exponential kernel. In *2013 IEEE Global Conference on Signal and Information Processing*, pp. 419–422.
- Hediger, S., L. Michel, and J. Näf (2022). On the use of random forest for two-sample testing. *Computational Statistics & Data Analysis* 170, 107435.
- Henze, N. (1988). A multivariate two-sample test based on the number of nearest neighbor type coincidences. *The Annals of Statistics* 16(2), 772–783.
- Henze, N. and M. D. Penrose (1999). On the multivariate runs test. *The Annals of Statistics* 27(1), 290–298.

- Johnson, A., L. Bulgarelli, L. Shen, A. Gayles, A. Shammout, S. Horng, T. Pollard, S. Hao, B. Moody, B. Gow, L.-w. Lehman, L. Celi, and R. Mark (2023, 01). Mimic-iv, a freely accessible electronic health record dataset. *Scientific Data* 10, 1.
- Kenter, T. and M. De Rijke (2015). Short text similarity with word embeddings. In *Proceedings of the 24th ACM International on Conference on Information and Knowledge Management*, pp. 1411–1420.
- Kim, I., A. Ramdas, A. Singh, and L. Wasserman (2021). Classification accuracy as a proxy for two-sample testing. *The Annals of Statistics* 49, 411–434.
- Li, J. (2018). Asymptotic normality of interpoint distances for high-dimensional data with applications to the two-sample problem. *Biometrika* 105(3), 529–546.
- Li, S.-Y., Y. Jiang, and Z.-H. Zhou (2014). Partial multi-view clustering. In *Proceedings of the AAAI Conference on Artificial Intelligence*, Volume 28.
- Little, R. J. A. (1992). Regression with missing x’s: A review. *Journal of the American Statistical Association* 87(420), 1227–1237.
- Lopez-Paz, D. and M. Oquab (2017). Revisiting classifier two-sample tests. In *International Conference on Learning Representations*.
- Mas-Celis, F., J. Olea-Lopez, and J. A. Parroquin-Maldonado (2021). Sepsis in trauma: a deadly complication. *Archives of Medical Research* 52(8), 808–816.
- Mueller, S., M. Weiner, L. Thal, R. Petersen, C. Jack, W. Jagust, J. Trojanowski, A. Toga, and L. Beckett (2005a, November). The alzheimer’s disease neuroimaging initiative. *Neuroimaging Clinics of North America* 15(4), 869–877.
- Mueller, S., M. Weiner, L. Thal, R. Petersen, C. Jack, W. Jagust, J. Trojanowski, A. Toga, and L. Beckett (2005b, July). Ways toward an early diagnosis in alzheimer’s disease: The alzheimer’s disease neuroimaging initiative (adni). *Alzheimer’s and Dementia* 1(1), 55–66.
- Pan, W., Y. Tian, X. Wang, and H. Zhang (2018, 06). Ball divergence: Nonparametric two sample test. *The Annals of Statistics* 46, 1109–1137.

- Rosenbaum, P. R. (2005). An exact distribution-free test comparing two multivariate distributions based on adjacency. *Journal of the Royal Statistical Society Series B: Statistical Methodology* 67(4), 515–530.
- Ross, R., A. Breskin, and D. Westreich (2020, 06). When is a complete case approach to missing data valid? the importance of effect measure modification. *American Journal of Epidemiology* 189.
- Schilling, M. F. (1986). Multivariate two-sample tests based on nearest neighbors. *Journal of the American Statistical Association* 81(395), 799–806.
- Singer, M., C. S. Deutschman, C. W. Seymour, M. Shankar-Hari, D. Annane, M. Bauer, R. Bellomo, G. R. Bernard, J.-D. Chiche, C. M. Coopersmith, et al. (2016). The third international consensus definitions for sepsis and septic shock (sepsis-3). *Journal of the American Medical Association* 315(8), 801–810.
- Song, H. and H. Chen (2024). Generalized kernel two-sample tests. *Biometrika* 111(3), 755–770.
- Toutenburg, H. (1990, 12). Rubin, d.b.: Multiple imputation for nonresponse in surveys. *Statistical Papers - STAT PAP* 31, 180–180.
- Wang, Q., Z. Ding, Z. Tao, Q. Gao, and Y. Fu (2018). Partial multi-view clustering via consistent gan. In *2018 IEEE International Conference on Data Mining*, pp. 1290–1295. IEEE.
- Xu, C., D. Tao, and C. Xu (2015). Multi-view learning with incomplete views. In *IEEE Transactions on Image Processing*, Volume 24, pp. 5812–5825. IEEE.
- Xue, F. and A. Qu (2021). Integrating multisource block-wise missing data in model selection. *Journal of the American Statistical Association* 116(536), 1914–1927.
- Zeng, Y., N. M. Adams, and D. A. Bodenham (2024a). MMD two-sample testing in the presence of arbitrarily missing data. *arXiv preprint arXiv:2405.15531*.
- Zeng, Y., N. M. Adams, and D. A. Bodenham (2024b). On two-sample testing for data with arbitrarily missing values. *arXiv preprint arXiv:2403.15327*.
- Zhang, C., Y. Cui, Z. Han, J. T. Zhou, H. Fu, and Q. Hu (2020). Deep partial multi-view learning. In *IEEE Transactions on Pattern Analysis and Machine Intelligence*, Volume 44, pp. 2402–2415. IEEE.



- Zhang, Z. (2016, 02). Missing data imputation: Focusing on single imputation. *Annals of Translational Medicine* 4, 9.
- Zhao, H., H. Liu, and Y. Fu (2016). Incomplete multi-modal visual data grouping. In *Proceedings of the International Joint Conference on Artificial Intelligence*, pp. 2392–2398.
- Zhou, D., T. Cai, and J. Lu (2023). Multi-source learning via completion of block-wise overlapping noisy matrices. *Journal of Machine Learning Research* 24(221), 1–43.
- Zhou, D. and H. Chen (2023). A new ranking scheme for modern data and its application to two-sample hypothesis testing. In *The Thirty Sixth Annual Conference on Learning Theory, 12-15 July 2023, Bangalore, India*, Volume 195 of *Proceedings of Machine Learning Research*, pp. 3615–3668. PMLR.